

# Numerical Investigation and Experimental Validation of Different Air Flow Conditioners using Up - and Down - Stream Pipeline

M. Štefanič<sup>†</sup> and A. Lipej

University of Novo mesto Faculty of Mechanical Engineering, Novo mesto, 8000, Slovenia

<sup>†</sup>Corresponding Author Email: [matej.stefanic@fs-unm.si](mailto:matej.stefanic@fs-unm.si)

(Received September 20, 2022; accepted January 28, 2023)

## ABSTRACT

The purpose of this study is to determine whether it is possible to reduce the upstream and downstream length of a measuring pipeline by installing different types of air flow conditioners. The main goal is to investigate the distance position of these flow conditioners and thus analyze their impact on flow conditions within the pipeline. To improve the current conditions in the pipeline, an analysis was performed of how measurement accuracy was impacted by installing different types of air flow conditioners. Measurement accuracy would also be improved. The preliminary analysis included two different types of flow conditioners: Zanker and NEL. Both were inserted into a measuring pipeline for measuring velocity field and profiles, and thus reduce uncertainty during measurements. A CFD model was built for each type of the air flow conditioner that simulated its impact on velocity fields in the measuring pipeline using the ANSYS Fluent software package. Numerical results of velocity profiles were validated and compared with experimental result. The Zanker flow conditioner was selected for the installation in the measuring pipeline due to better results compared to NEL. Based on the numerical results, the air flow conditioner was optimized and the most suitable conditioner was selected, in this case *D/10-V3*.

**Keywords:** Air flow conditioner; CFD, Pitot- Prandtl tube; Velocity profile; Optimization.

## NOMENCLATURE

$C$	coefficient of discharge	$R$	diameter
$D$	distance	$q_{mid}$	ideal mass flow rate
$d$	diameter	$R$	diameter
$\vec{F}$	force vector	$t$	time
$\vec{g}$	gravitational acceleration	$\vec{v}$	velocity vector
$K$	pressure loss coefficient	$\alpha$	outflow number
$p$	pressure	$\beta$	diameter ratio
$p_d$	pressure difference	$\varepsilon$	expansibility factor
$p_s$	static pressure	$\rho$	fluid density
$p_t$	total pressure	$\bar{\tau}$	stress tensor
$q_m$	mass flow rate	$\nabla$	nabla
$q_{mid}$	ideal mass flow rate	$y^+$	non dimensional

## 1. INTRODUCTION

In many applications, flow and velocity sensors are needed during fluid flow in pipelines. They are used for measuring the flow of water, industrial gas, oil or steam. There are several methods of measuring fluid flows, such as obstruction method (orifice meter, flow nozzle, Venturi tube), pressure difference method (Pitot-Prandtl tube), vortex, thermal, turbine,

ultrasonic, Coriolis and electromagnetic method, and volumetric method. The flow meter is selected according to the required application. The obstruction method of measuring flows is a classic method in which the measurement effect is based on the change in static pressure due to the change in the flow area. The pressure difference method uses the Pitot-Prandtl tube, which is used to measure the local

velocity. For this method, a developed velocity profile is necessary. There are certain solutions to achieve better measurement results. Problems due to the undeveloped velocity profile are also noticeable with the obstruction flow meters, such as the orifice meter. Due to these problems, air flow conditioners are used to create better flow conditions in the pipeline. The advantage of installing flow conditioners is also to reduce the length of the pipeline, but an appropriate distance between the flow meter and the air flow conditioner must be found. The downside of the flow conditioner is additional pressure losses due to the installation. The field is described in the standard ISO 5167-1 (ISO-5167-1 2003; ISO-5167-2 2003a). Conditioners should be installed at a position such that the pipe flow is fully developed. The required upstream and downstream straight length is specified with  $D$ , which represents the distance between the downstream face of the conditioner and the flow meter. In the case of flow meters in pipelines, measurement errors may occur due to an undeveloped velocity profile in the pipeline, mainly due to insufficient upstream and downstream length of the pipeline (VDI/VDE 2041 1991). The standard describes the conditions of the installation in the pipelines and provides information on the calculation of the flow and measurement uncertainty. In this research, the velocity measurement uncertainty was reduced by designing velocity profiles when using the Pitot-Prandtl tube by using air flow conditioners.

One of the sources investigated was the impact of air flow conditioners on the measurement accuracy of the fluid flow. This is a general research about air flow conditioners that does not take into account the Zanker or NEL conditioners. It also does not cover the different installation distances. However, it gives a basic insight into the velocity profiles (Sawchuk *et al.* 2010). Another source describes the Zanker conditioner, which was used to study the flow swirling at different distances. They concluded that Zanker is very useful and gives good results in a wide range of the Reynolds number on different distances of the installation. They recommend a distance of 7.5  $D$  from the obstruction element (also recommended in ISO 5167-1). It is useful for different pipeline diameters and in a wide range of the Reynolds numbers (Zanker and Goodson 2000). In the third source, similar research on measuring velocity profiles was done using the Doppler laser velocimetry. They ran tests with the Zanker and NEL conditioners. An undeveloped velocity profile was detected at specified distances (Hinz *et al.* 2016). Our basic source of information was therefore the standard ISO 5167 (ISO-5167-1 2003; ISO-5167-2 2003a), which provides detailed information and guidance on the use of air flow conditioners, and ISO 3966 (ISO-3966 2020), which guides the use of the Pitot-Prandtl tube. As stated in the standard, precise positioning of the Pitot-Prandtl tube is required for accurate measurements. This study is focused on the use of numerical analyses and turbulence models. The first turbulent model for turbulence modelling was the Realizable  $k - \varepsilon$  model (RKE). This model also uses wall functions to inventory the boundary layer. This also results in more accuracy in the

rotational flow, boundary layers, pressure gradients and flow separation (Shih *et al.* 1995). To obtain boundary layers, the Enhanced Wall Treatment wall function, which makes the model more suitable in a wider range of the non-dimensional variable  $y^+$ , was selected (ANSYS 2016). The second turbulent model for turbulence modelling was  $k - \omega$  SST (Shear Stress Transport), which represents a compromise between the ordinary model  $k - \omega$  and model Realizable  $k - \varepsilon$  and has the properties of both models (Menter 1994). In this model, variable  $\varepsilon$  is replaced by variable  $\omega$ , illustrating the specific dissipation of turbulent energy. The model better describes the flow movement in the viscous layer, results are more accurate in separation, transitions, flow collisions and lower values of the Reynolds number. The model is accurate and robust for flow in the viscous layer with high pressure gradients. To capture the boundary layer, we can use the wall function. The viscous layer is calculated with the model  $k - \omega$ , and the outer layers (free flow) are calculated using the model  $k - \varepsilon$  (ANSYS 2016). The third turbulent model for turbulence modelling was  $k - kl - \omega$ , which shows the ability of the model to describe transitional flow behaviour with good accuracy, in comparison with commonly used models that have no capability of predicting the boundary layer development (Walters and Cokljat 2008). The last turbulent model was *Transitional SST*. It is based on the  $k - \omega$  SST model and is used where a significant proportion of the boundary layer is laminar, mostly in aerodynamics and turbomachinery (Menter *et al.* 2004).

In the study, a numerical analysis was performed to investigate the possibility of installing air flow conditioners in the pipeline. The goal was to reduce the length of the pipe by correctly setting the distance position of the air flow conditioners and optimizing the flow conditioners. To improve the current conditions in the pipeline, the impact on the measurement results was analyzed. The preliminary analysis comprises two different flow conditioners, i.e. Zanker and NEL flow conditioners. The obtained numerical results were validated with experimental results. For the positioning of the Pitot-Prandtl tube, a robot was used.

## 2. NUMERICAL ANALYSIS

### 2.1 Numerical Model and Mesh

For numerical simulations, the RANS turbulent modelling approach was used. The SIMPLE scheme and second order solvers were used. Second order discretization schemes are mainly used with tetra mesh, where the substance or flow is not aligned with the grid and flows aslant through the cell of the mesh, so the discretization of equations in the first order discretization scheme may result in a numerical error (ANSYS 2016).

Governing equations of fluid dynamics are conservation of mass and momentum for incompressible flow (ANSYS 2016):

$$\frac{\partial \rho}{\partial t} + \nabla \cdot (\rho \vec{v}) = 0 \tag{1}$$

$$\begin{aligned} \frac{\partial}{\partial t}(\rho \vec{v}) + \nabla \cdot (\rho \vec{v} \vec{v}) \\ = -\vec{\nabla} p + \nabla \cdot (\vec{\tau}) \\ + \rho \vec{g} + \vec{F} \end{aligned} \tag{2}$$

The computational domain was divided into different volumes, thus gaining the possibility of better control over the preparation of the computational mesh. The domain was divided into six volumes with a separate district nozzle and air flow conditioner and a separate part with an area representing the distance of measurement with the Pitot-Prandtl measuring probe. Two symmetries were taken into account, namely on the surface of the YZ and on the surface of the ZX, which represent an advantage by significantly reducing the number of final volumes, since only 1/4 tubes are taken into account. The numerical model was simulated with two symmetries to cover 1/4 of the model. The numerical domain was divided into 6 volumes with a separate orifice plate and air flow conditioner allowing for better control of the mesh and individual parts of the domain. A combination of tetrahedrons and hexahedrons was used, therefore this meshing method can significantly reduce the number of volumes. Tetrahedrons were applied to more complex geometries and hexahedrons were applied to geometrically less complex parts of the domain. Fig. 1 shows the computational domain and boundary condition.

Fig. 2 shows a mesh of air flow conditioners, Zanker (left) and NEL (right).

Due to its geometric simplicity, the mesh is mostly made with hexahedrons, allowing a lower number of volumes for the same mesh quality, and the tetrahedrons are used around the orifice plate and

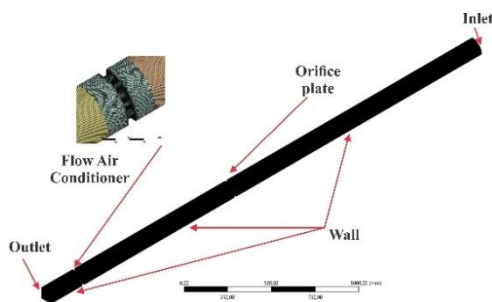


Fig. 1. Computational domain.

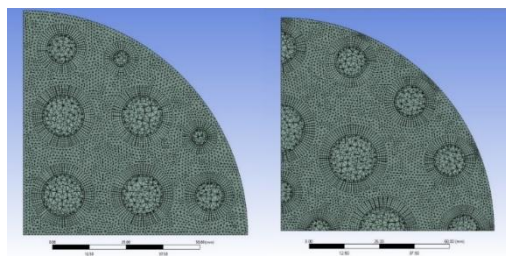


Fig. 2. Side view of mesh on the flow conditioner.

Table 1  $y^+$  of the mesh ( $k - \omega SST$  and  $Tk - kl - \omega$ )

		$k - \omega SST$		
		$y^+_{ave}$	$y^+_{min}$	$y^+_{max}$
Zanker	6 D	0,32	$1,8 \times 10^{-3}$	3,2
	7 D	0,32	$1,9 \times 10^{-3}$	3,2
	8 D	0,32	$9,7 \times 10^{-4}$	3,2
NEL	6 D	0,32	$1,7 \times 10^{-3}$	3,2
	7 D	0,32	$4,2 \times 10^{-4}$	3,2
	8 D	0,32	$9,8 \times 10^{-4}$	3,2
		$Tk - kl - \omega$		
		$y^+_{ave}$	$y^+_{min}$	$y^+_{max}$
Zanker	6 D	0,37	0,005	3,2
	7 D	0,37	0,005	3,2
	8 D	0,37	0,006	3,2
NEL	6 D	0,38	0,0048	3,2
	7 D	0,38	0,0063	3,2
	8 D	0,38	0,0048	3,2

conditioner. To make a good inventory of the boundary layer, the inflation function and additional local mesh settings around the surfaces or bodies were used. The basic mesh covers the entire domain and was used in all models, including the one where only the inflation function is used to obtain the boundary layer, thus achieving the correct  $y^+$  values. Based on previous analyses and research on this application and the measuring pipeline, it is concluded that the number of elements is sufficient. The main criterion for mesh and the use of the right turbulent model was thus the value  $y^+$ . By refining the mesh, the solution was independent of the computational mesh. The final mesh had 3.5 million finite volumes (Realizable  $k - \epsilon$ , *ewt*) and 15 million finite volumes ( $k - \omega SST$ , *Tk kl - omega*, *Transitional SST*).

The difference in the divergence of finite volumes is in the turbulence models. Low-Reynolds turbulence models such as  $k - \omega SST$  for boundary layers require  $y^+$  below 1, so the grid in the boundary layer must be dense enough. However, for turbulent models with wall functions such as the  $k - \epsilon$  model, this condition is not required. This means that the boundary regions are calculated with wall functions. The quality of the mesh is also important, so it is necessary to check aspect ratio, skewness and orthogonal quality. These conditions make a difference in the mesh.

The value of  $y^+$  is important. The  $y^+$  values are shown in the table (Table 1 and Table 2).

## 2.2 Boundary Condition

It is important to determine the boundary conditions for the correct inventory of the numerical domain. The boundary condition of symmetry was also used on the two planes of the model, which divides the domain into a quarter. This reduced the number of final volumes and consequently also the computational time. The boundary condition of the speed inflow into the domain was determined, namely 4.56 m/s and 5.33 m/s, and a pressure output without overpressure of 0 Pa. The air density was set at  $1.1536 \text{ kg/m}^3$  and the air viscosity at  $1.57065 \times 10^{-4}$

**Table 2**  $y^+$  of the mesh (Realizable  $k - \epsilon$ , ewt and Transitional SST)

		Realizable $k - \epsilon$ , ewt		
		$y^+_{ave}$	$y^+_{min}$	$y^+_{max}$
Zanker	6 D	5,4	0,06	26,5
	7 D	5,7	0,04	23,7
	8 D	5,3	0,06	26,5
NEL	6 D	5,3	0,07	26,5
	7 D	5,7	0,07	31
	8 D	5,3	0,04	26,5
		Transitional SST		
		$y^+_{ave}$	$y^+_{min}$	$y^+_{max}$
Zanker	6 D	0,36	0,004	3,3
	7 D	0,36	0,005	3,3
	8 D	0,35	0,003	3,3
NEL	6 D	0,33	0,001	3,3
	7 D	0,34	0,002	3,8
	8 D	0,34	0,002	3,8

<sup>5</sup> kg/ms, corresponding to the results of the measurements.

### 3. EXPERIMENTAL ANALYSIS

With air flow conditioners, flow swirling was prevented, the distortion of the velocity profile was reduced and symmetry of the fluid velocity profile was achieved, which helps reduce the measurement errors of velocity and fluid flows. The advantage of installing the conditioners is also in reducing the required upstream length of the straight part of the pipeline while defining the appropriate distance between the flow meter and the conditioner. The downside of the air flow conditioner are additional pressure losses due to the installation. When using obstruction methods of flow or velocity measurement, the dimensionless value  $K$  is defined, which represents a pressure loss for a particular part in the pipeline, which may be a conditioner or, for example, an orifice. The pressure loss coefficient can be expressed from the pressure difference equation Eq. (3) (ISO-5167-1 2003):

$$\Delta p = \frac{K \cdot \rho \cdot v^2}{2} \quad (3)$$

The orifice plate is classified as an obstruction method of fluid flow measuring. The plate narrows the flow channel, so the flow is suffocated, resulting in a difference in static pressures  $\Delta p$  in front of the plate (static pressure  $p_1$ ) and behind the plate (static pressure  $p_2$ ). The fluid flow is calculated using the equation Eq. (4) (VDI/VDE 2041 1991):

$$q_m = q_{mid} C \epsilon = \frac{C}{\sqrt{1 - \beta^4}} \epsilon \frac{\pi \cdot d^2}{4} \cdot \sqrt{2 \Delta p \rho} \quad (4)$$

$$= \alpha \epsilon \frac{\pi \cdot d^2}{4} \cdot \sqrt{2 \Delta p \rho}$$

The Pitot-Prandtl tube is based on the pressure method. The shape of the pipe is designed to have a minimal impact on velocity vectors and is considered one of the most widely used velocity measurement methods. The advantages of the Pitot-Prandtl tube are insensitivity, robustness and low price compared

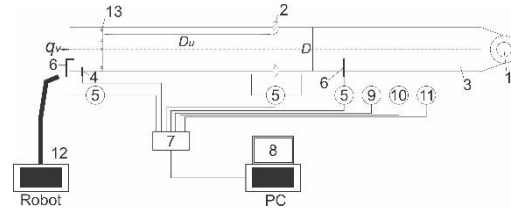


**Fig. 3.** Measuring line.

to other measurement methods, and easy measurement. The Pitot-Prandtl tube measures the local velocity based on the pressure difference.

The measurement uncertainty of the Pitot-Prandtl tube at a 95% confidence level is less than 2%, usually 1.5% (ISO-3966 2020). Velocity is obtained using the equation Eq. (5) (ISO-3966 2020):

$$w = \sqrt{\frac{2(p_t - p_s)}{\rho}} = \sqrt{\frac{2p_d}{\rho}} \quad (5)$$

The measurements were carried out at predetermined distances of 5.25 mm between points. The positioning of the Pitot-Prandtl measuring probe was carried out using a robot that was programmed to follow a predetermined path. The repeatability of the robot is 0.02 mm (Robotics 2019). All measurements were fully automated and there was no need to interfere with the measuring range or otherwise affect the course of the measurements during the measurement itself. This has eliminated external influences. The robot was programmed to measure one point for 2 + 15 seconds. This means that the robot passed the distance to the measurement point, waited two seconds and performed a measurement that lasted 15 seconds. Then the next cycle was performed at the next point. The Pitot-Prandtl measuring probe was positioned so that the tip of the probe was moved 33 mm inside the pipeline. The velocity measurement uncertainty is 2.7% and the flow 1.7%.

A customized measuring line was used to analyze the implementation of air flow conditioners in the laboratory where the flow conditions was analyzed Fig. 3.

- |     |                       |     |                             |
|-----|-----------------------|-----|-----------------------------|
| 1.  | ventilator,           | 2.  | orifice plate,              |
| 3.  | pipe,                 | 4.  | Pitot - Prandtl tube (PPT), |
| 5.  | pressure converter,   | 6.  | temperature sensor,         |
| 7.  | data logger,          | 8.  | PC,                         |
| 9.  | environment pressure, | 10. | temperature sensor,         |
| 11. | hygrometer,           | 12. | robot.                      |
| 13. | air flow conditioner, |     |                             |

### 3.1 Velocity Profiles

Figure 4, Fig. 5 and Fig. 6 show the velocity profiles of the Zanker conditioner at different distances: 6 D, 7 D and 8 D. All velocity profiles are symmetrical. For all three installations, the velocity profile was created.

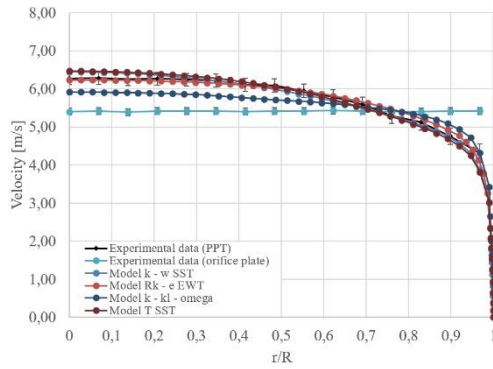


**Fig. 4. Velocity profile Zanker 6 D.**

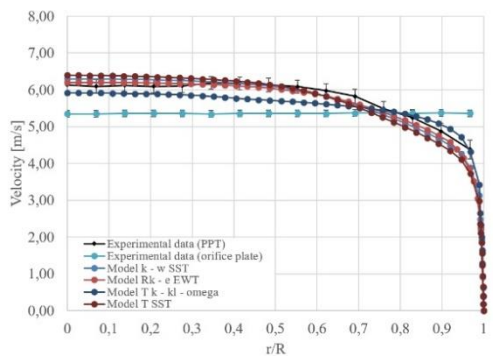


**Fig. 5. Velocity profile Zanker 7 D.**

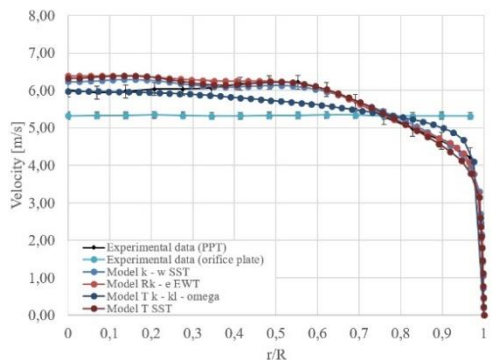


**Fig. 6. Velocity profile Zanker 8 D.**

At a distance of 6 D, the maximum difference is present with the model  $k - kl - \omega$ , which shows a lower velocity between 0 and 0.6 R, while in the area between 0.75 R and 1 R, this model has a higher velocity. Other models are showing a smaller difference. The model  $k - \omega$  SST has a slightly higher velocity. A smaller difference is noticeable between distances 0 and 0.3 R. The difference occurs mainly in approaching the wall of the pipe.

At a distance of 7 D, there are small differences between the models. The model  $k - kl - \omega$  has deviation across the whole area.

At a distance of 8 D, a slight difference between the distances 0 and 0.5 R is observed, where the  $k - kl - \omega$  model has lower velocity while other models have slightly higher velocity. The difference occurs mainly in approaching the wall of the pipe.

Figure 7, Fig. 8 and Fig. 9 show the velocity profiles of the NEL conditioner at different distances: 6 D, 7 D, and 8 D. All velocity profiles are symmetrical. A velocity profile was created for all three installations.

With the NEL conditioner, a slightly larger deviation between the turbulent models is obtained. Velocity is slightly lower with the Realizable  $k - \epsilon$ ,  $\epsilon WT$  model at distances between 0 and 0.3 R in all three distances. A lower velocity of 0 to 0.5 R is revealed also with the  $k - kl - \omega$  model.

At a distance of 8 D, there is also a difference in the wall of the pipe, or at distances of 0.8 to 1 R. There is also a distortion of the velocity profile at a distance of 7 D, mainly at a distance of 8 D, where distinctive points are observed at distances of 0 R and 0.35 R.

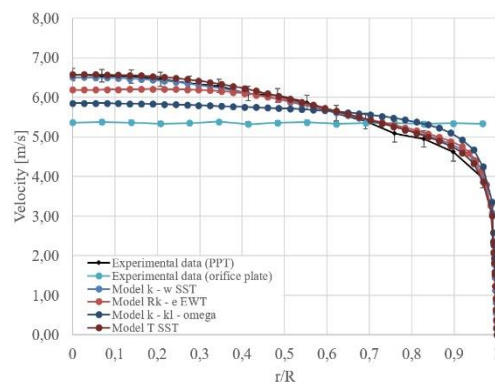


**Fig. 7. Velocity profile NEL 6 D.**

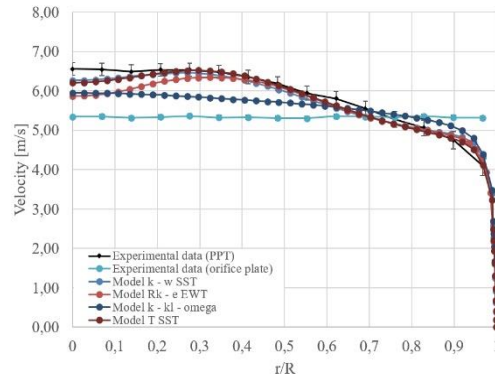


**Fig. 8. Velocity profile NEL 7 D.**

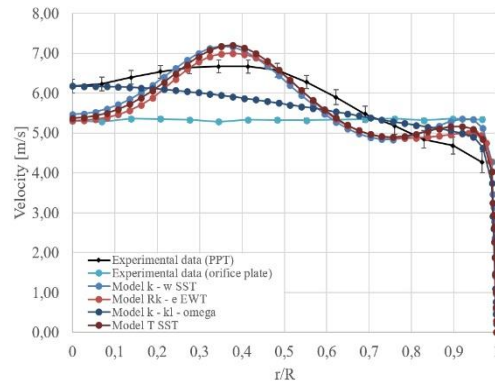


**Fig. 9. Velocity profile NEL 8 D.**

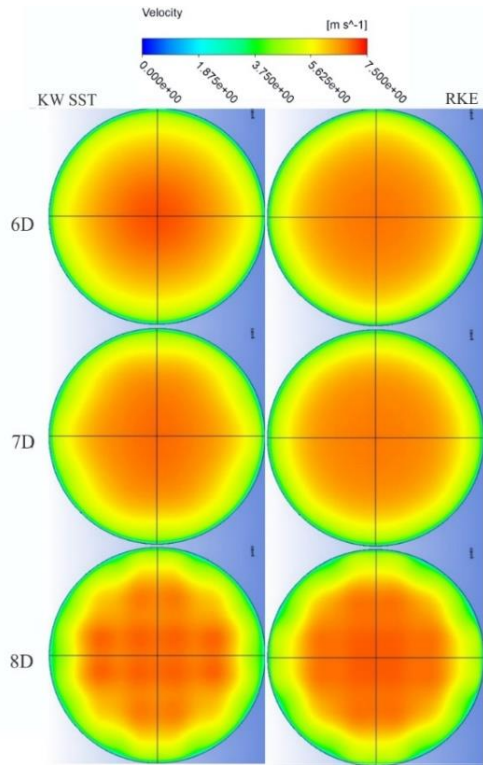


Fig. 10. Comparison of velocity between turbulent models (Zanker).

### 3.2 Contour of Velocity and Turbulent Kinetic Energy

The contours for velocity and turbulent kinetic energy are shown with a comparison between the Realizable  $k - \epsilon$ ,  $\epsilon_{wt}$  and  $k - \omega$  SST turbulent models, which are recommended for standard cases (ANSYS 2016).

Figure 10 shows a comparison of the Zanker flow conditioner. A slightly more homogeneous velocity field is observed when using the Realizable  $k - \epsilon$ ,  $\epsilon_{wt}$  turbulent model, while the model  $k - \omega$  SST has a slightly less homogeneous velocity field. The larger difference is observed mainly when positioning the conditioner at a distance of 8 D. The higher value of velocity when using the Realizable  $k - \epsilon$ ,  $\epsilon_{wt}$  model can be attributed to the properties of the turbulent model, such as different adherence to the boundary layer. Realizable  $k - \epsilon$ ,  $\epsilon_{wt}$  is not a low Reynolds turbulent model compared to  $k - \omega$  SST.

Figure 11 shows a comparison of the NEL flow conditioner. The Realizable  $k - \epsilon$ ,  $\epsilon_{wt}$  turbulent model has a more homogeneous velocity field. However, a marked high velocity field is observed in the circle in the middle of the pipe. This was already observed in the previous section when reviewing velocity profiles.

Figure 12. shows a comparison of turbulent kinetic energy for Zanker. It is a more homogeneous field with the Realizable  $k - \epsilon$ ,  $\epsilon_{wt}$ .

Figure 13 shows a comparison of turbulent kinetic energy for NEL. The turbulent model  $k - \omega$  SST has

bigger differences in the turbulence field. With the Realizable  $k - \epsilon$ ,  $\epsilon_{wt}$ , we get a more homogeneous field.

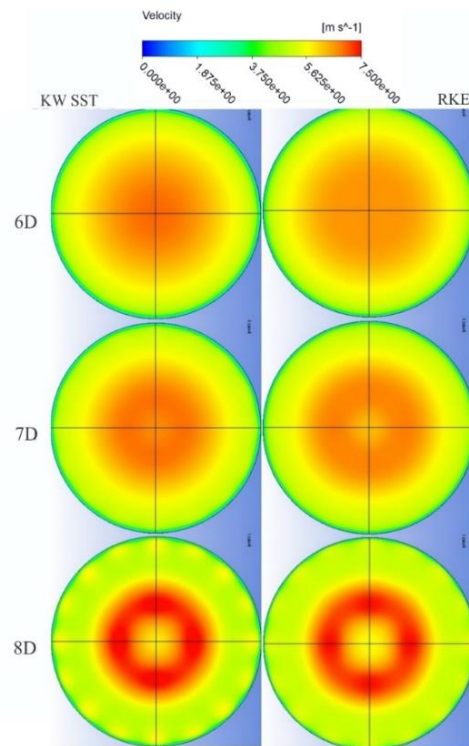


Fig. 11. Comparison of velocity between turbulent models (NEL).

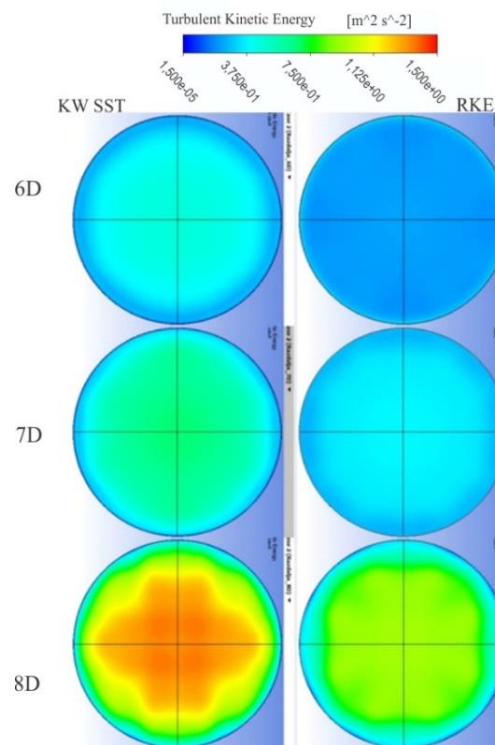


Fig. 12. Comparison of turbulent kinetic energy (Zanker).

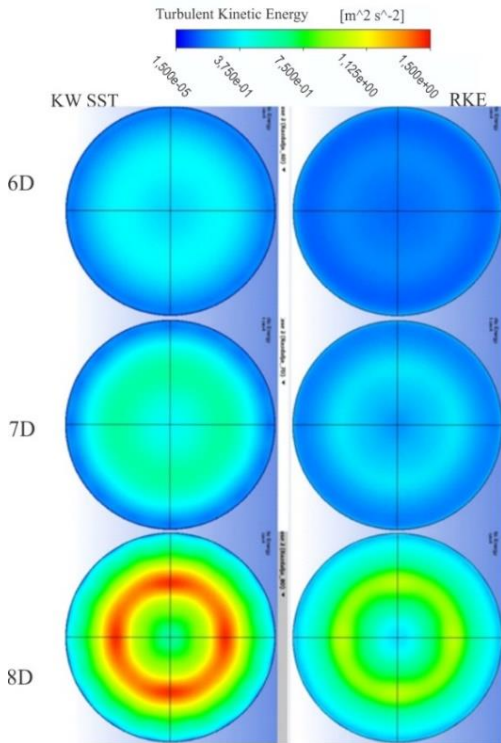


Fig. 13. Comparison of turbulent kinetic energy (NEL).

### 3.3 Optimization of the Air Flow Conditioner

By optimization, the mass of the conditioner was reduced, thus allowing savings as to the price and time of the manufacturing, while maintaining the velocity profile of the air and the pressure difference according to the basic Zanker conditioner with a thickness of D/8. The optimization conditions were unchanged air velocity profile and equal or smaller pressure difference compared to the original conditioner. Optimization was performed with the Realizable  $k - \epsilon$ ,  $ewt$  model. Fig. 14 shows the optimization of the thickness of the conditioner. There are no differences in the velocity profile between the different thicknesses of the conditioner.

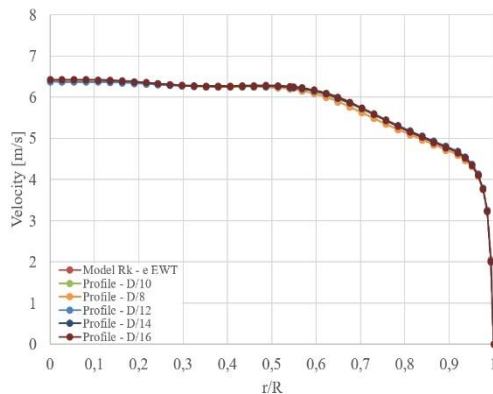


Fig. 14. Thickness effect on the velocity profile (Zanker 8D).

Table 3 Thickness impact on the pressure difference

Model	$D$ [mm]	$p_1$ [Pa]	$p_2$ [Pa]	$dp$ [Pa]	$K$
D/8	19	55,79	-7,98	63,76	4,3
D/10	15,2	54,81	-8,35	63,16	4,2
D/12	12,67	55,29	-8,70	63,99	4,3
D/14	10,85	56,28	-9,46	65,74	4,4
D/16	9,5	57,79	-10,76	68,55	4,6

Table 4 Standard deviation on the surface of the measurements

Standard deviation	D/8	D/10	Diff. [%]
Velocity [m/s]	1,323	1,303	1,5
Pressure [Pa]	0,014	0,014	0
TKE [m <sup>2</sup> /s <sup>2</sup> ]	0,257	0,258	0,4

The choice of the air flow conditioner was followed by the pressure difference. Table 3 shows the pressure differences according to the thickness of the conditioner. Since the pressure difference is minimal, a conditioner D/10 with a thickness of 15.2 mm was selected. This reduced the dimensions of the conditioner by 20%, which does not affect the characteristics of the conditioner itself. Pay attention to the interpretation of the results, as the pressure differences are small and can be attributed to a numerical error of the computational mesh. However, the D/10 air flow conditioner was selected.

A comparison of the standard deviation on the surface of the measurement with the Pitot - Prandtl tube ensued (Table 4). The customized D/10 conditioner shows better results relative to the original version with a thickness of D/8 and original hole diameter. The standard deviation of the velocity was reduced by 1.5%, pressure and the turbulent kinetic energy (TKE) stay the same.

Figure 15 shows the velocity field of the optimized V1-D/10 conditioner, where the velocity field is homogeneous and the maximum velocity difference is 0.15%.

After the initial iteration of the optimization, an approach test followed to the point of the measurement with the Pitot - Prandtl tube at a 1 D distance. The velocity profiles are shown in Fig. 16. A distortion of the air velocity profile is observed, so a test was conducted to optimize the impact of the

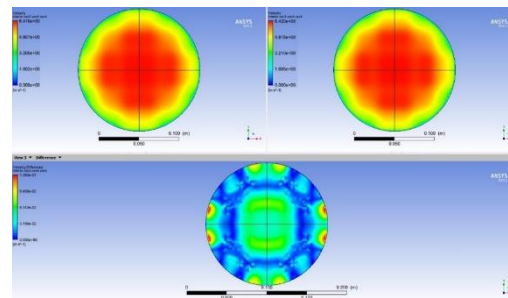
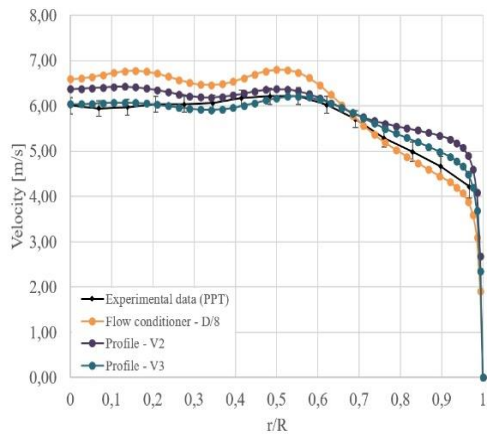


Fig. 15. Velocity field of the optimized flow conditioner V1.



**Fig. 16. Velocity profiles of the optimized flow conditioner V1.**

diameter of the holes on the air velocity profile. With two versions of the conditioner with new hole diameters, we also improved the velocity profile of the air. Good results are mainly evidenced by the D/10-V3 conditioner, which tracks experimental measurements with minimal deviations. The slightly larger deviation is only on the edge, where we get a slightly higher velocity.

Table 5 shows the results of the pressure comparison between the conditioners D/8 and D/10-V3. Otherwise, we get a slightly larger pressure difference and a coefficient of pressure loss.

The adjusted air flow conditioner D/10-V3 is based on a Zanker conditioner with dimensions that depend on the diameter of D:

- a) 4 holes diameter  $d_1$ ,  $0.120 R \pm 0.001 R$ , pitch circle diameter  $0.25 R \pm 0.0025 R$ ,
- b) 8 holes diameter  $d_2$ ,  $0.118 R \pm 0.001 R$ , pitch circle diameter  $0.56 R \pm 0.0056 R$ ,

- c) 4 holes diameter  $d_3$ ,  $0.123 R \pm 0.001 R$ , pitch circle diameter  $0.75 R \pm 0.0075 R$ ,

- d) 8 holes diameter  $d_4$ ,  $0.101 R \pm 0.001 R$ , pitch circle diameter  $0.85 R \pm 0.0085 R$ ,

- e) 8 holes diameter  $d_5$ ,  $0.069 R \pm 0.001 R$ , pitch circle diameter  $0.90 R \pm 0.009 R$ .

The standard deviation on the surface of the measurement with the Pitot - Prandtl tube was compared (Table 6). The customized conditioner D/10-V3 shows better results compared to the original version with a thickness of D/8 and the original diameter of the holes.

The standard deviation of the velocity was reduced by 14%, the pressure by 27% and the turbulent kinetic energy (TKE) by less than 1%.

The D/10-V3 conditioner also has a more homogeneous velocity field compared to the D/8 conditioner. The maximum velocity of 10% was also reduced. A comparison of contours is shown in Fig. 17.

**Table 5. Pressure comparison**

Model	$D$ [mm]	$p_1$ [Pa]	$p_2$ [Pa]	$dp$ [Pa]	$K$
D/8	19	99,85	14,46	114,31	7,7
D/10-V3	15,2	116,74	19,04	135,78	9,1

**Table 6 Comparison of standard deviation on the location (surface) of the measurements**

Standard deviation	D/8	D/10-V3	Diff. [%]
Velocity [m/s]	1,559	1,341	14
Pressure [Pa]	0,089	0,070	27
TKE [m <sup>2</sup> /s <sup>2</sup> ]	0,917	0,909	0,88

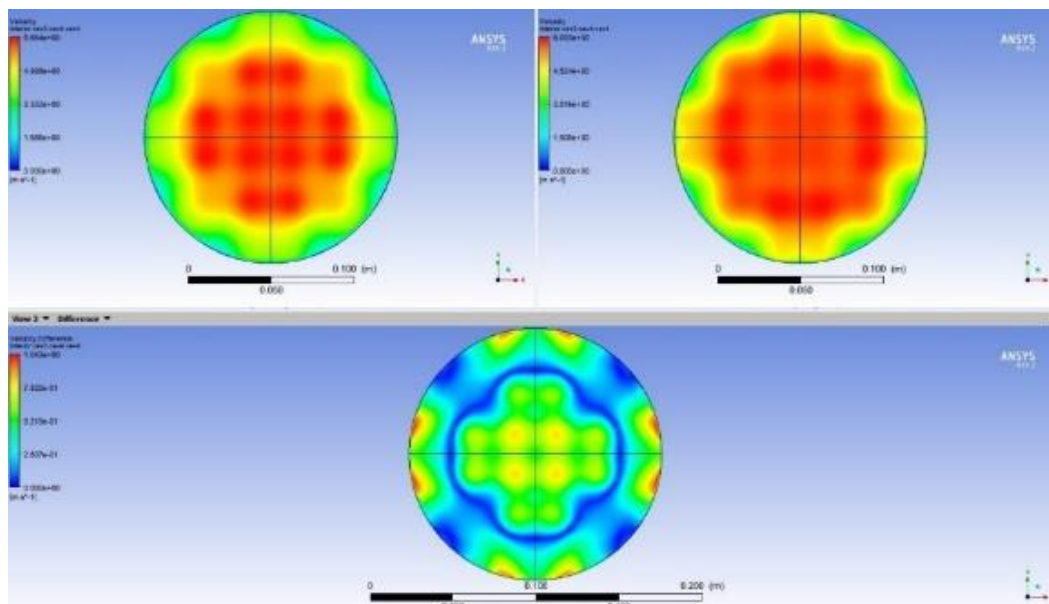


**Fig. 17. Velocity field of the optimized flow conditioner D/10-V3.**

## 5. CONCLUSION

In the research, the flow conditions in the pipeline with integrated air flow conditioners using computational fluid dynamics with experimental validation were examined. In the experimental analysis a robot was used, for accurate positioning, and consequently ensured very good repeatability of the measurements with the Pitot - Prandtl tube. For the modelling turbulence,  $k - \omega$  SST and Realizable  $k - \varepsilon$  showed good results.

Based on the validation of the results, the Zanker air flow conditioner showed better results and provided a developed velocity profile at all flows and distances. Based on the results and validations obtained, the best air flow conditioner would be Zanker at a distance of 8 D. It has a homogeneous velocity field, a developed velocity profile and sufficient recommendations for positioning the conditioner at a distance  $L_s$ :  $7,5 \leq L_s \leq 8,5 D$  (ISO-5167-2 2003b).

In the process of optimization during the first research phase, a conditioner with a thickness of  $D/10$  showed the best results. In the second research phase of the optimization, the  $D/10$ -V3 conditioner was selected, which showed better results relative to the homogeneity of the velocity and turbulent field compared to the Zanker conditioner, and a better velocity profile. Based on the experimental and numerical results obtained, our expectations for the use of air flow conditioners to improve the flow conditions in the pipeline of the measuring line can be confirmed.

Future research will include some hybrid or URANS turbulence models which have advantages over RANS and LES turbulence methods (Bézar *et al.* 2011; Menter 2012). One of these is the Scale Adaptive Simulation SAS (Menter and Egorov 2010) and Detached eddy simulation DES (Spalart *et al.* 2006). The URANS hybrid models, such as DES and SAS models, are based on the RANS method in the boundary layer and the transition to the LES method in external separation regions. They were developed for the massive separation of flows in aerodynamics.

## REFERENCES

- ANSYS (2016). *ANSYS Fluent Theory Guide*. ANSYS Inc.
- Bézar, H., B. Chauat, F. Chedevergne, S. Deck and E. Laroche (2011). Transition and Turbulence Modeling. *Journal of Aerospace Lab* (2), 1-13.
- Hinz, D. F., S. Graner and C. Breitsamter (2016). Conditioning of swirling and stratified pipe-flow: analysis with laser-doppler velocimetry. In *FLOMEKO*, Sydney, Australia.
- ISO-3966 (2020). Measurements of fluid flow in closed conduits- Velocity Area Method Using Pitot Static Tubes. 39.
- ISO-5167-1 (2003). Measurement of fluid flow by means of pressure differential devices- Part 1: Orifice Plates, Nozzles and Venturi Tubes Inserted in Circular Cross-Section Conduits Running Full. 81.
- ISO-5167-2 (2003a). Measurement of fluid flow by means of pressure differential devices- Part 1: Orifice Plates, Nozzles and Venturi Tubes Inserted in Circular Cross-Section Conduits Running Full. 47.
- ISO-5167-2 (2003b). Measurements of fluid flow by means of pressure differential devices inserted in circular cross-section conduits running full- Part 2: Orifice Plates.
- Menter, F. R. (1994). Two-equation eddy-viscosity turbulence models for engineering applications. *AIAA Journal* 32(8), 1598-1605.
- Menter, F. R. (2012). Best practice : scale-resolving simulations in ANSYS CFD. *ANSYS Germany GmbH* 1-70.
- Menter, F. R. and Y. Egorov (2010). The scale-adaptive simulation method for unsteady Turbulent Flow Predictions. Part 1: Theory and Model Description. *Flow, Turbulence and Combustion* 85(1), 113-138.
- Menter, F. R., R. B. Langtry, S. R. Likki, Y. B. Suzen, P. G. Huang and S. Völker (2004). A correlation-based transition model using local variables—part i: model formulation. *Journal of Turbomachinery* 128(3), 413-422.
- Robotics, A. B. B. (2019) *Product Specification IRB 1200*. Document ID: 3HAC05960-001 Revision: Q.
- Sawchuk, B. D., D. P. Sawchuk and D. A. Sawchuk (2010). Flow conditioning and effects on accuracy for fluid flow measurement. *American School of Gas Measurement Technology* 1-9.
- Shih, T. H., W. W. Liou, A. Shabbir, Z. Yang and J. Zhu (1995). A new  $K-\varepsilon$  eddy viscosity model for high reynolds number turbulent flows. *Computers & Fluids* 24(3), 227-238
- Spalart, P. R., S. Deck, M. L. Shur, K. D. Squires, M. Kh. Strelets and A. Travin (2006). A new version of detached-eddy simulation, resistant to ambiguous grid densities. *Theoretical and Computational Fluid Dynamics* 20(3), 181.
- VDI/VDE 2041 (1991). Measurement of fluid flow with primary devices; orifice plates and nozzles for special applications.
- Walters, D. K. and D. Cokljat (2008). A three-equation eddy-viscosity model for reynolds-averaged navier–stokes simulations of transitional flow. *Journal of Fluids Engineering* 130(12), 121401.
- Zanker, K. and D. Goodson (2000). Qualification of a flow conditioning device according to the new API 14.3 procedure. *Flow Measurement And Instrumentation* 11(2), 79-87.